Science and Technology Indonesia
e-ISSN:2580-4391 *p*-ISSN:2580-4405
Vol. 9, No. 3, July 2024

Research Paper

Synthesis and Characterization of Perovskite Manganate Based on $La_{0.7}Ca_{0.3}MnO_3$ with Ni and Ti doping as Microwave Absorber Material

Sitti Ahmiatri Saptari[1]*, Mufidatul Mar'ah[1], Yana Taryana[2], Nanang Sudrajat[3]

[1]*Department of Physics, Universitas Islam Negeri Syarif Hidayatullah Jakarta, Tangerang Selatan, Banten, 15412, Indonesia*
[2]*Research Center for Telecommunication, National Research and Innovation Agency, Bandung, Jawa Barat, 40135, Indonesia*
[3]*Research Center for Advanced Material, National Research and Innovation Agency, Bandung, Jawa Barat, 40135, Indonesia*
***Corresponding author**: sitti.ahmiatri@uinjkt.ac.id

Abstract
Research has been carried out on the effect of Ni and Ti doping on the microwave absorption properties of the perovskite manganate material $La_{0.7}Ca_{0.3}Mn_{1-x}Ni_{x/2}Ti_{x/2}O_3$ (LCMNTO) with variations x = 0; 0.03; 0.05; and 0.1, which were synthesized by the sol-gel method. The effect of Ni and Ti doping on the structure, grain size, magnetic properties, and microwave absorption properties were investigated in detail by various analytical methods. XRD (x-ray diffraction) characterization showed that the material $La_{0.7}Ca_{0.3}Mn_{1-x}Ni_{x/2}Ti_{x/2}O_3$ has a single phase with an orthorhombic crystal system. The SEM (scanning electron microscope) results showed a tendency to decrease in grain size when the composition of Ni and Ti dopants began to increase. VSM (vibrating sample magnetometer) characterization shows that $La_{0.7}Ca_{0.3}Mn_{1-x}Ni_{x/2}Ti_{x/2}O_3$ is a soft magnet with magnetic properties that decrease with increasing Ni and Ti dopant composition. The characterization of VNA (vector network analyzer) in the 8-12 GHz shows that the highest ability to absorb microwaves is 98% at 8.24 GHz, and there is an addition of absorption areas point and widening of the absorption bandwidth. Thus, the material $La_{0.7}Ca_{0.3}Mn_{1-x}Ni_{x/2}Ti_{x/2}O_3$ has the potential to become a microwave absorber material.

Keywords
$La_{0.7}Ca_{0.3}Mn_{1-x}Ni_{x/2}Ti_{x/2}O_3$, Sol-Gel Method, Microwave Absorber

Received: 21 February 2024, Accepted: 29 April 2024
https://doi.org/10.26554/sti.2024.9.3.577-585

1. INTRODUCTION

The COVID-19 pandemic that has hit the world since 2019 created a new normal condition, which causes an increase in the daily need for electronic devices, wireless communication devices, local area networks, and so on that use microwaves in the frequency range 1-20 GHz, such as laptop and handphone used in the online school learning, and work from home (WFH). The increasing use of electromagnetics at various, exceptionally high frequencies, which is increasingly intensive in line with technological developments, causes electromagnetic wave interference, reducing the device's performance (Akinay et al., 2023). In addition, long-term exposure to electromagnetic radiation can hurt health. Anil's research stated that at least 60% of microwave radiation is absorbed and penetrates the area around the head and can cause health problems in parts of the body, including the reproductive, nervous, and psychological systems (Saradva, 2023).

Electromagnetic wave absorber material can convert electromagnetic wave energy into heat energy, which helps protect an object from unwanted electromagnetic waves (Zhang et al., 2022). Therefore, many researchers are researching to engineer or obtain materials with the best absorption capabilities. Microwave absorber material performs well intrinsically and has good magnetic and electrical properties. Structure modification on lanthanum manganese by doping on the La site and Mn site with the form $La_{(1-x)}AE_xMn_{(1-y)}TM_yO_3$ (AE = divalent ions such as Ca^{2+}, Sr^{2+}, Ba^{2+}; TM = transition metal ions such as Cu, Fe, Ni, Co, Ti) will lead to exchange interactions that can affect the magnetic and electrical properties of the material (Akram et al., 2023; Dimri et al., 2021; González García et al., 2023; Keshri et al., 2021; Mu et al., 2022; Suresh et al., 2023). Liu et al. (2018) researched the absorption properties of microwaves at $La_{1-x}Ca_xMnO_3$ and obtained a reflection loss value of -42 dB at x = 0.1 with a bandwidth of 3.5 GHz. In another study, substituting transition metals in LSMO increased the ability to absorb microwaves (Zhang and Cao, 2012). Adi and Manaf Ridwan (2017) substituted Fe and Ti ions in LBMO and found that the combined doping of Fe and Ti increased the reflection loss and improved performance.

Materials synthesized using the sol-gel method have a ho-

mogeneous size distribution and physical properties of materials that increased in the results of previous studies (Alabada et al., 2023; Çoban Özkan et al., 2021; Ye et al., 2022; Zheng et al., 2023). Cheng et al. (2005) reported a 10 K increase in curie temperature in LCMO materials synthesized using the sol-gel method, Ts = 773 K. Taşarkuyu et al. (2011) reported an increase in curie temperature in LCMO double perovskite material and a rise in the temperature sintering. In this research, the selection of Ti and Ni ions as doping content at the Mn site is based on the following considerations: First, it has been reported by Rizky et al. (2022) that they researched the microwave absorption properties in $La_{0.7}Ca_{0.3}Mn_{1-x}Ti_xO_3$ synthesized using the sol-gel method. That, along with the increase in the composition of the Ti dopant, causes the magnetic properties to decrease. The same results were reported in the Hua et al. study, which analyzed the influence of Ni doping on the magnetic and magnetocaloric properties of LCMO materials. With the Ni doping, the contents of Mn^{3+} and Mn^{4+} change, weakening the double exchange interaction (Hua et al., 2013). Second, double doping of Ti and Ni in perovskite $La_{0.7}Sr_{0.3}Mn_{1-x}(Ni,Ti)_{x/2}O_3$ has been reported by Saptari et al. (2022), with space group (R-3c), the presence of Ti and Ni doping does not change its basic crystal structure. Furthermore, the higher the content of Ti and Ni, the more it improves its absorption ability from -3.572 dB at x = 0.1 to -11.8 dB at x = 0.5.

Furthermore, Several studies have conducted various analyses on LCMO substituted with Ti ions or other transition metals at the Mn site. However, no reports of LCMO analysis substituted Ni and Ti (LCMNTO) have been found. This paper is aimed to analyze the crystal structure, morphology, grain size, magnetic properties, and performance of $La_{0.7}Sr_{0.3}Mn_{1-x}(Ni,Ti)_{x/2}O_3$ (x = 0; 0.03; 0.05; and 0.1) synthesized using the sol-gel method (Ts = 1200°C) as a microwave absorber material. Therefore, the research on the combined doping of Ni and Ti in LCMO holds high significance that can fill the knowledge gap in the study of new perovskites. The results of this research are expected to provide a deeper insight into more optimal microwave absorber materials, thereby contributing to the development of perovskite-based technology.

2. EXPERIMENTAL SECTION

2.1 Materials

Samples of $La_{0.7}Ca_{0.3}Mn_{1-x}Ni_{x/2}Ti_{x/2}O_3$ (x = 0; 0.03; 0.05; and 0.1) were synthesized by the sol-gel method using some raw materials. The materials were La_2O_3 (Merck 99%), $Ca(NO_3)_2.4H_2O$ (Merck 99%), $Mn(NO_3)_2.4H_2O$ (Merck 98.5%), TiO_2 (Merck 99%), $Ni(NO_3)_2.6H_2O$ (Merck 99%), $C_6H_8O_7 \cdot H_2O$ (Merck 99.5%), nitric acid 65% (HNO_3), ammonia solution 25%, aquabidest, and alcohol 70%.

2.2 Instrumentations

The sample's phase composition, crystal system, and crystal grain size were measured using X-ray diffraction (XRD). This test was carried out at the XRD Laboratory of Research Center for Telecommunication, National Research and Innovation Agency, Bandung, using the PANalytical brand with Cu anode (λ=1.54056 Å), Empyrean type, scanning angle at 15°-90° with step size 0.02°. The sample used in this test is a powder placed in the sample testing area on the XRD. This x-ray diffraction (XRD) data will then be analyzed by matching the data using software, and qualitative refinement was carried out using the GSAS software. A Scanning Electron Microscope (SEM) examined sample morphology and grain size distribution. This test was carried out at the Research Center for Telecommunication, National Research and Innovation Agency Bandung, with magnifications of 1000, 3000, 5000, 10000, and 20000.

The magnetic properties of the samples were checked using a Vibrating Sample Magnetometer (VSM). This test was conducted at the Physics Research Center (P2F-BRIN) Serpong. The information obtained from this characterization is magnetization parameters due to changes in the external magnetic field described in the hysteresis curve. Finally, the material absorption properties and reflection loss values will be obtained using the Vector Network Analyzer (VNA) characterization. This test was conducted at the Research Center for Electronics and Telecommunications, National Research and Innovation Agency (PRISTEK-BRIN) Bandung with the emitted frequency range of 8-12 GHz, the X-band microwave frequency. The material's absorption property is the ability to absorb electromagnetic waves emitted by a wave transmitter at a specific frequency range. At the same time, reflection loss is caused by the process of reflecting electromagnetic waves that hit the sample.

2.3 Methods

The synthesis of perovskite manganese material using the sol-gel method is expected to produce a high-purity and homogeneous material (Navas et al., 2021). In the sample preparation step, the mass of the precursor material was weighed according to stoichiometric calculations, while citric acid was used as a catalyst. The next step consists of two processes, namely, the hydrolysis process and the gelatin process. The hydrolysis process began with the nitrate solution from each precursor mixed and stirred using a magnetic stirrer until homogeneous. After that, the solution was stirred while heated to a temperature of ± 180°C until the solution had a temperature of ± 70°C. Next is the gelatin process, where the solution is added to ammonia until the solution's pH is seven and is in the form of a gel. In the dehydration step, the gelled sample was heated in an oven at 200°C for ± 1.5 hours. After that, the sample (dry-gel) was pulverized using a mortar and transferred to a crucible cup to enter the calcination heating step using a furnace at a temperature of 600°C for 6 hours, which will remove organic compounds in the sample. After that, the samples were mashed again with mortar, and the next step was sintering with a furnace at a temperature of 1200°C for 6 hours for sample crystallization. The samples in the furnace were pulverized using a mortar and sieve no. 200 and tested for XRD, SEM, VSM, and VNA characterization.

Table 1. Refinement Results of Materials $La_{0.7}Ca_{0.3}Mn_{1-x}Ni_{x/2}Ti_{x/2}O_3$ (x = 0; 0.03; 0.05; and 0.1)

Parameter	$La_{0.7}Ca_{0.3}Mn_{1-x}Ni_{x/2}Ti_{x/2}O_3$			
	x = 0	x = 0.03	x = 0.05	x = 0.1
Space Group		Pnma		
Crystal System		Orthorhombic		
a (Å)	5.4645	5.4637	5.4656	5.4672
b (Å)	7.7232	7.7219	7.7249	7.7274
c (Å)	5.4808	5.4796	5.4814	5.4829
V ($Å^3$)	231.31	231.18	231.43	231.64
Density (g/cm^3)	6.093	6.095	6.088	6.080
Strain (10^{-5})	36.6	43.8	78.5	80
Crystallite Size (nm)	133.65	110.92	142.00	92.44
Discrepancy Factors				
RwP (%)	10.6	9.43	9.41	9.21
Rp (%)	8.47	7.54	7.46	7.32
Bond lengths (Å)				
Mn−O(1)	1.96468(4)	1.96434(3)	1.96512(4)	1.96573(5)
Mn−O(2)	1.95746(3)	1.96124(3)	1.96190(3)	1.96246(4)
<Mn−O>	1.96107(3)	1.96279(8)	1.96351(4)	1.96410(0)
Bond angles (°)				
Mn−O(1)−Mn	158.6886(5)	158.6895(5)	158.6909(6)	158.6917(8)
Mn−O(2)−Mn	161.7988(3)	161.7987(3)	161.7980(3)	161.7977(4)
<Mn−O−Mn>	160.2437(4)	160.2441(0)	160.2445(5)	160.2447(6)
Bandwidth (a.u)				
W (10^{-2})	9.327977	9.299405	9.287480	9.277805
Tolerance Factor				
Goldschmidt	0.9075112	0.907047	0.906737	0.905964

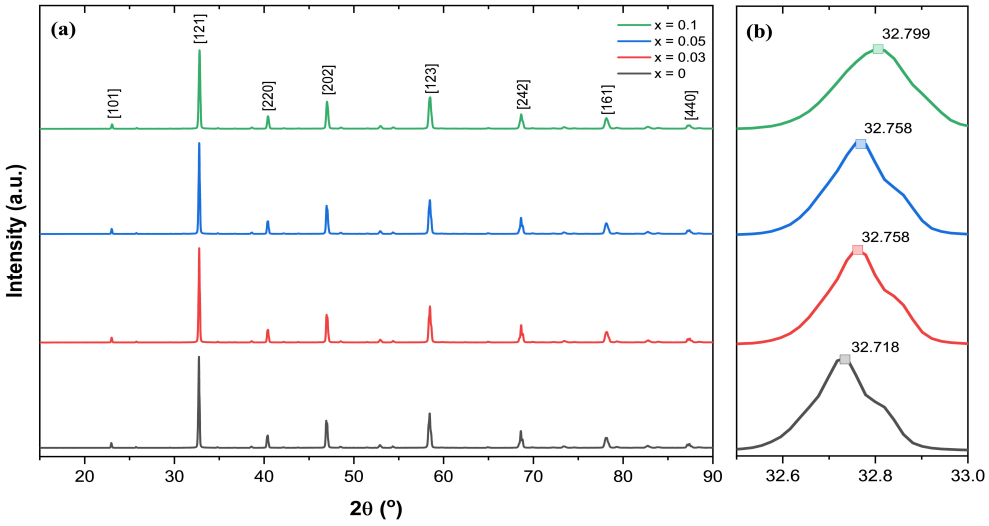

Figure 1. (a) XRD Pattern of $La_{0.7}Ca_{0.3}Mn_{1-x}Ni_{x/2}Ti_{x/2}O_3$ (x = 0; 0.03; 0.05; and 0.1), (b) Peak Shift at 2θ ~32.7°.

3. RESULTS AND DISCUSSION

3.1 Crystal Structure

The XRD characterization was carried out at room temperature, and the data were analyzed using the Rietveld method. The resulting diffraction pattern shows that the increase in the substitution of Ni and Ti ions (x = 0; 0.03; 0.05; 0.1) causes a change in intensity and a shift in peak position without changing the XRD pattern (Figure 1). He et al. (2024) stated that this 2θ shift indicated that there had been a replacement of cations in the compound lattice. So, in this study, the intensity and peak

Table 2. Comparison of Refinement Results of Materials $La_{0.7}Ca_{0.3}Mn_{1-x}Ni_{x/2}Ti_{x/2}O_3$ (x = 0; 0.03; 0.05; and 0.1) to other similar references perovskite structure.

Perovskites	Space Group	Lattice Parameters (Å) a	b	c	V (Å^3)	References
$La_{0.7}Ca_{0.3}MnO_3$	Pnma	5.4645	7.7232	5.4808	231.31	This work
$La_{0.7}Ca_{0.3}Mn_{0.97}Ni_{0.015}Ti_{0.015}O_3$	Pnma	5.4637	7.7219	5.4796	231.18	This work
$La_{0.7}Ca_{0.3}Mn_{0.95}Ni_{0.025}Ti_{0.025}O_3$	Pnma	5.4656	7.7249	5.4814	231.43	This work
$La_{0.7}Ca_{0.3}Mn_{0.9}Ni_{0.05}Ti_{0.05}O_3$	Pnma	5.4672	7.7274	5.4829	231.64	This work
$La_{0.7}Ca_{0.3}MnO_3$	Pnma	5.4517	7.7280	5.4653	230.26	(Hua et al., 2013)
$La_{0.7}Ca_{0.3}Mn_{0.95}Ni_{0.05}O_3$	Pnma	5.4479	7.7319	5.4692	230.38	(Hua et al., 2013)
$La_{0.7}Ca_{0.3}Mn_{0.9}Ni_{0.1}O_3$	Pnma	5.4410	7.7040	5.4630	229.50	(Hua et al., 2013)
$La_{0.7}Ca_{0.3}Mn_{0.7}Ti_{0.3}O_3$	Pm-3m	3.8762	3.8762	3.8762	58.24	(Rizky et al., 2022)
$La_{0.7}Ca_{0.3}Mn_{0.95}Ti_{0.05O3}$	Pnma	5.4932	7.7623	5.4988	234.47	(Ulyanov et al., 2006)

Table 3. The Average Grain Size of Sample $La_{0.7}Ca_{0.3}Mn_{1-x}Ni_{x/2}Ti_{x/2}O_3$ Based on SEM Results

Doping Concentrate x	Grain Average Size (μm)
0	0.899
0.03	1.168
0.05	1.130
0.1	1.098

position change indicated that Ni and Ti are doping at the site Mn. In the XRD pattern, no typical peaks were found due to the doping of Ni and Ti. This is because the doping of Ni and Ti is still within an acceptable tolerance of $La_{0.7}Ca_{0.3}MnO_3$ and can replace Mn well in the perovskite LCMO structure. This result is from a study conducted by Saptari et al., who reported that the diffraction pattern of $La_{0.7}Sr_{0.3}Mn_{1-x}(Ni, Ti)_{x/2}O_3$ obtained for all variations of the value of x showed the same diffraction pattern, indicated by the peaks at nearly the same 2θ angle (Saptari et al., 2022). The results of the data analysis are summarized in Table 1. The analysis results in Table 1 provide information that the material $La_{0.7}Ca_{0.3}Mn_{1-x}Ni_{x/2}Ti_{x/2}O_3$ (x = 0; 0.03; 0.05; and 0.1) is a single-phase with the same crystal system and space group for the four samples, namely orthorhombic (Pnma). In addition, we compare the results of lattice parameter XRD refinement with various research similar perovskite compositions in Table 2 and show structural similarities for the minimum Mn doping site content. The Goldschmidt tolerance factor (τ_G) calculation for all samples calculated based on Equation (1), which is $\tau_G \approx 0.91$, based on the research of Ardani et al. (2021), when $r < 0.96$, the perovskite will have an orthorhombic crystal.

$$\tau_G = \frac{0.7r_{La^{3+}} + 0.3r_{Ba^{2+}} + r_{O^{2-}}}{\sqrt{2\left[(0.7-x)r_{Mn^{3+}} + 0.3r_{Mn^{4+}} + 0.5xr_{Ti^{3+}} + r_{O^{2-}}\right]}} \quad (1)$$

In addition, these results also show that there is a change in lattice parameters without the difference in the crystal system, causing a change in the bond length <Mn−O> and the bond angle <Mn−O−Mn>, which affects the material's bandwidth. The decrease in the value of bandwidth (W) and the increase in lattice strain, along with the addition of Ni and Ti dopants compositions, have an impact on reducing the strength of the double exchange (DE) interaction between Mn^{4+} and Mn^{3+} and will cause a super-exchange that can decrease in magnetic properties (Bouzidi et al., 2019).

3.2 Morphology and Grain Size

The morphological results obtained show polygonal and some circular grains in the four samples shown in Figure 2. These results are based on the morphological images of materials with orthorhombic crystal systems attached to several previous studies, namely pentagonal or hexagonal grains (Karoblis et al., 2020; Xu et al., 2019). Table 3 shows that the samples not doped with Ni and Ti have the smallest grain size. Then, after doping Ni and Ti (x = 0.03), the grain size increases drastically and then decreases again with the increase in dopant concentration. Based on the results of XRD analysis, the grain size obtained is much larger than the crystallite size, so the material $La_{0.7}Ca_{0.3}Mn_{1-x}Ni_{x/2}Ti_{x/2}O_3$ (x = 0; 0.03; 0.05; and 0.1) is polycrystalline. The grain size in polycrystalline affects the electron transfer process in the material. The smaller grain size leads to the larger intergrain, with the tunnelling and electron transfer processes being more complex, so the resistivity in the material will be greater (Kurniawan et al., 2019).

3.3 Magnetic Properties

Properties of material $La_{0.7}Ca_{0.3}Mn_{1-x}Ni_{x/2}Ti_{x/2}O_3$ (x = 0; 0.03; 0.05; and 0.1) is known from the results of the VSM characterization in the form of a hysteresis curve (Figure 3) which shows that at room temperature $La_{0.7}Ca_{0.3}Mn_{1-x}Ni_{x/2}Ti_{x/2}O_3$ (x = 0; 0.03; 0.05; and 0.1) is a ferromagnetic material. A similar curve shape was found in Reddy et al. (2011)'s research, which showed a hysteresis curve of ferromagnetic polyvinylidene fluoride (PVDF) composite film, which is straight at the end but has loops around the coordinate points. Zhang et al. (2011) also obtained a curve with a similar loop in the $Co_{0.7}Fe_{2.1}O_4$ ferromagnetic. Ferromagnetic materials have a

Table 4. Material Magnetization Parameter Data $La_{0.7}Ca_{0.3}Mn_{1-x}Ni_{x/2}Ti_{x/2}O_3$

Doping x	Ms (emu/g)	Mr (emu/g)	Hc (Oe)	Loop Area (KOe.emu/g)
0	9.58	0.03	81.71	0.9
0.03	6.29	0.02	100.34	0.5
0.05	5.14	0.02	121.9	448.5
0.1	3.83	0.02	116.14	333.7

Table 5. Results on the Percentage of Microwave Absorption Ability on Materials $La_{0.7}Ca_{0.3}Mn_{1-x}Ni_{x/2}Ti_{x/2}O_3$ (x = 0; 0.03; 0.05; 0.1)

Doping x	Frequency (GHz)	Reflection Loss (dB)	Through Power (%)
0	8.24	-18.00	98.42
	9.50	-9.32	88.30
	11.20	-3.20	52.14
0.03	8.42	-17.40	98.18
	9.54	-12.80	94.75
	11.20	-4.40	63.70
0.05	8.66	-8.74	86.63
	9.68	-12.10	93.83
	11.36	-6.88	79.49
0.1	8.92	-5.71	73.15
	9.68	-9.12	87.75
	10.42	-6.37	76.93
	11.04	-8.40	85.55

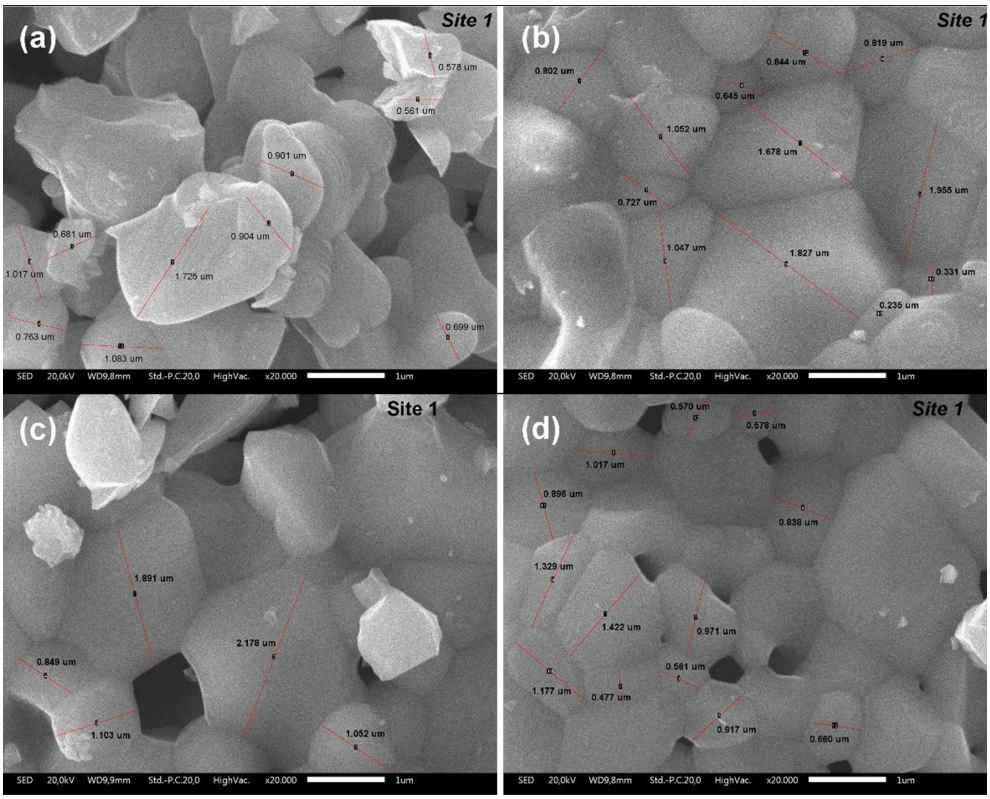

Figure 2. Morphological Results of SEM $La_{0.7}Ca_{0.3}Mn_{1-x}Ni_{x/2}Ti_{x/2}O_3$ with (a) x = 0 (b) x = 0.03 (c) x = 0.05 (d) x = 0.1

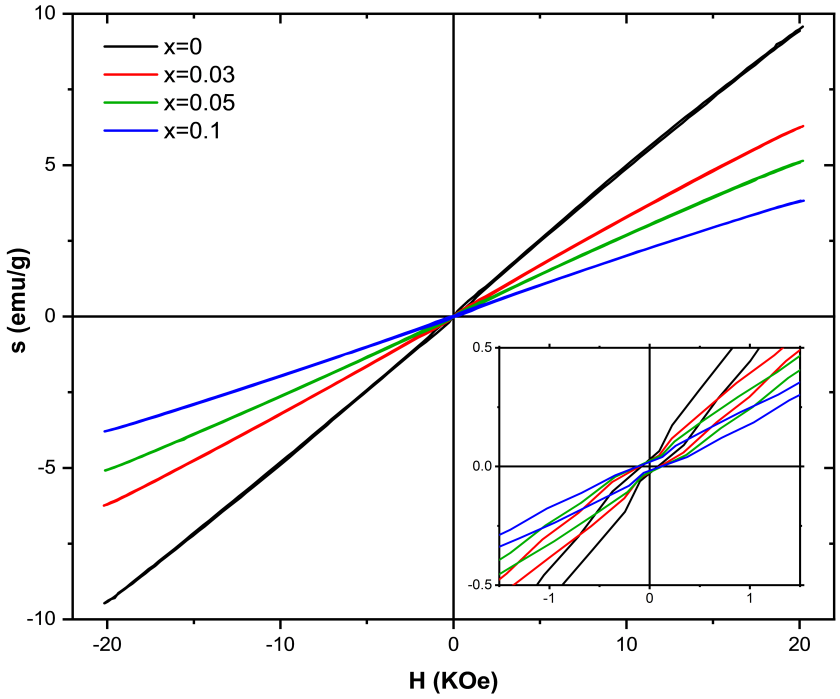

Figure 3. Hysteresis Curve $La_{0.7}Ca_{0.3}Mn_{1-x}Ni_{x/2}Ti_{x/2}O_3$ (x = 0; 0.03; 0.05; 0.1)

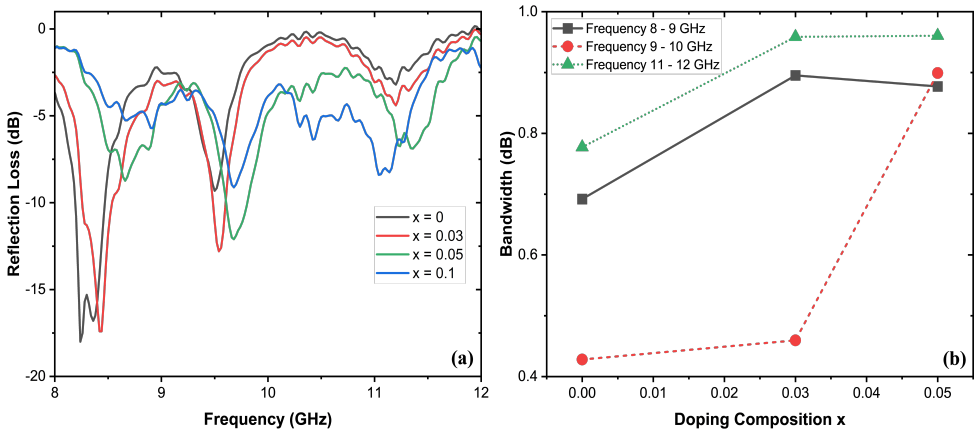

Figure 4. (a) Graph of the Combined Relationship of Reflection Loss with Frequency (b) Changes in Absorption Bandwidth Along with the Increase in the Composition of Ni and Ti

spontaneous magnetic moment even if they are in a zero external magnetic field or a hysteresis curve, i.e., a remanent field. This spontaneous magnetization indicates that the material's electron spin and magnetic moment are arranged regularly. The small coercivity field indicates that the four samples are soft magnetic (Khodayari and Gholizadeh, 2024).

The curve and magnetization parameter table (Table 4) also shows a decrease in magnetic properties and an increase in the composition of Ni and Ti dopants, which is indicated by a reduction in magnetic saturation. In LCMNTO, using the theory of conservation of mass and charge, Ni and Ti doping at the Mn site causes a decrease in the quantity of Mn^{3+}. It directly impacts the double exchange (DE) interaction and weakens the ferromagnetic coupling between Mn^{3+} and Mn^{4+}. This condition also causes the emergence of interactions that contribute directly to weakening the material's magnetic properties, namely super-exchange, which is antiferromagnetic (Cheng et al., 2023).

3.4 Absorbance

Characterization using VNA in this study is in the form of S11 data (reflection coefficient) from the source of electromagnetic waves, namely the RL (Reflection loss) value, which represents the ability of a material to absorb electromagnetic waves. The

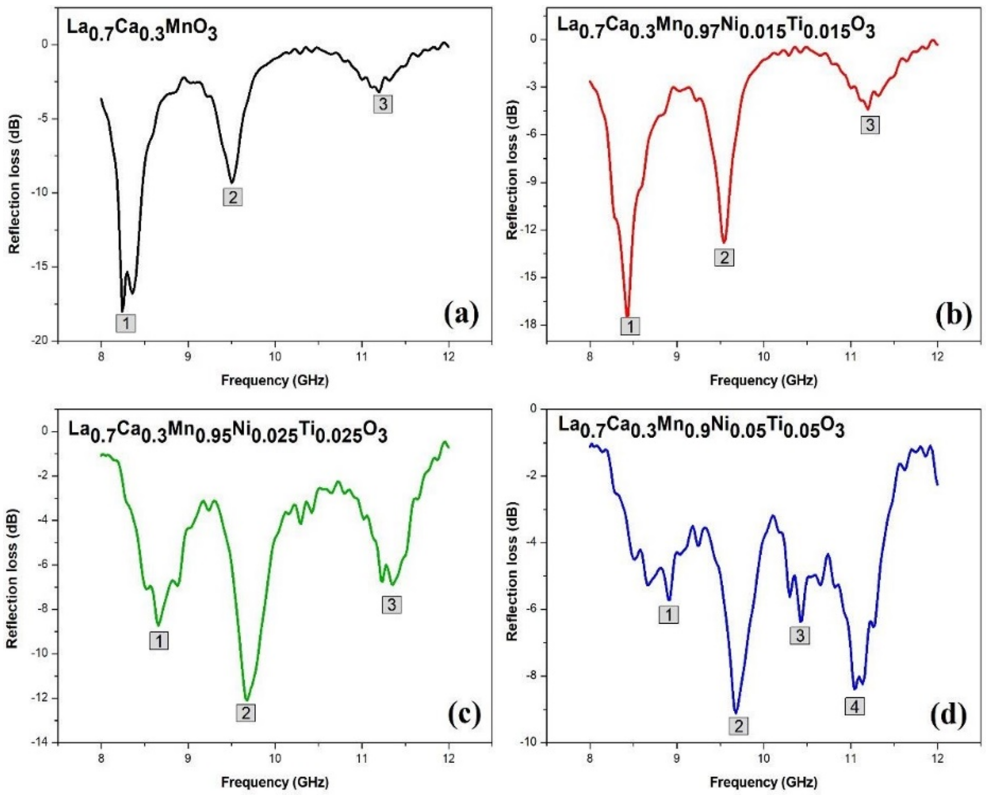

Figure 5. Graph of the relationship between Reflection Loss and frequency in $La_{0.7}Ca_{0.3}Mn_{1-x}Ni_{x/2}Ti_{x/2}O_3$ with (a) x = 0 (b) x = 0.03 (c) x = 0.05 (d) x = 0.1

frequency range used in this characterization is 8-12 GHz, the microwave frequency range (X-band). The characterization data is presented in Figure 4.

Each sample's combined Reflection Loss curve shows that the sample x = 0 has the deepest curve compared to the other samples. It indicates that the LCMO sample has the best ability to absorb microwaves in this study. In addition, it can also be seen that the maximum absorption point tends to shift to the right towards higher frequencies, and the absorption bandwidth gets broader as the composition of Ni and Ti dopants increases (Figure 4). In the 11-12 GHz frequency range, the absorption bandwidth of sample x = 0.1 is narrower because the LCMNTO sample (x = 0.1) has an additional absorption point area in the 10-11 GHz frequency range shown in Figure 5. It causes the utilization of LCMNTO material as an absorber to be more varied, so it can be used in several frequency ranges as needed. With the potential for shifting the absorption area to the right, it can reduce the negative impact of exposure to high-frequency radiation on the body.

Based on Table 5, which is the result of VNA data processing, Ni and Ti doping in LCMO reduces the ability of the material to absorb microwaves. This is due to the decreased magnetic properties of the material (Elmahaishi et al., 2022). In addition, the SEM results showed a decrease in grain size when the composition of Ni and Ti dopants began to increase. The smallest grain size in this study was owned by sample x = 0, namely samples that had not been doped with Ni and Ti. The smaller grain size would increase the material's resistivity (Bakonyi, 2021; Bishara et al., 2021; Mehner et al., 2020). Based on this, it is suspected that the electrical properties of the material have the potential to increase with the addition of Ni and Ti dopant compositions. However, at variations of x = 0, 0.03, 0.05, and 0.1, a decrease in magnetic properties dominates so that the material's ability to absorb microwaves continues to decrease.

4. CONCLUSION

Research on $La_{0.7}Ca_{0.3}Mn_{1-x}Ni_{x/2}Ti_{x/2}O_3$ (x = 0 0.03; 0.05; and 0.1), which was synthesized by the sol-gel method, was carried out. XRD analysis results show that LCMNTO is a single phase with the same crystal system and space group, orthorhombic (Pnma). Doping Ni and Ti cause changes in lattice parameters and bond lengths of Mn−O and bond angles of Mn−O−Mn so that there is a decrease in the bandwidth value, which can interfere with the double exchange. The results of SEM characterization showed a tendency to decrease in the average grain size when the Ni and Ti doping started to increase. In the VSM characterization test, all the samples are ferromagnetic materials with small coercivity values, so they are soft magnetic. The VSM results also showed a decrease in the ma-

terial's magnetic properties and an increase in the composition of Ni and Ti dopants, which was indicated by a decrease in the saturation field. In the VNA characterization results, Ni and Ti doping caused a decrease in the material's performance in absorbing microwaves. However, there was an increase in the absorption point areas and a widening of the absorption bandwidth. Thus, the material $La_{0.7}Ca_{0.3}Mn_{1-x}Ni_{x/2}Ti_{x/2}O_3$ has the potential to become a microwave absorber material at more varied frequencies.

5. ACKNOWLEDGMENT

The authors thank the Research Center for Telecommunication and the National Research and Innovation Agency for their support and instrumental analysis.

REFERENCES

Adi, W. A. and A. Manaf Ridwan (2017). Absorption Characteristics of the Electromagnetic Wave and Magnetic Properties of the $La_{0.8}Ba_{0.2}Fe_xMn_{1/2(1-X)}$ $Ti_{1/2(1-X)}O_3$ (x= 0.1-0.8) Perovskite System. *International Journal of Technology*, **5**(October); 887–897

Akinay, Y., U. Gunes, B. Çolak, and T. Cetin (2023). Recent Progress of Electromagnetic Wave Absorbers: A Systematic Review and Bibliometric Approach. *ChemPhysMater*, **2**(3); 197–206

Akram, M., M. Umair, M. A. Yaqub, S. M. Ramay, S. Naseem, and S. Atiq (2023). Nanostructured Fe-Substituted $LaMnO_3$ Perovskites as a High-Performance Electrode for Supercapacitors. *ECS Journal of Solid State Science and Technology*, **12**(9); 093005

Alabada, R., M. M. Kadhim, Z. sabri Abbas, A. M. Rheima, U. S. Altimari, A. H. Dawood, Z. T. Abed, R. S. Radhi, A. S. Jaber, and S. K. Hachim (2023). Investigation of Effective Parameters in the Production of Alumina Gel through the Sol-Gel Method. *Case Studies in Chemical and Environmental Engineering*, **8**(December); 100405

Ardani, A., S. A. Saptari, and A. Tjahjono (2021). Analysis the Increased of Nickel Substitution on Crystal Structure and Magnetic Properties of Lanthanum Barium Manganate Material. In *AIP Conference Proceedings*, volume 2382. AIP Publishing

Bakonyi, I. (2021). Accounting for the Resistivity Contribution of Grain Boundaries in Metals: Critical Analysis of Reported Experimental and Theoretical Data for Ni and Cu. *The European Physical Journal Plus*, **136**(4); 410

Bishara, H., S. Lee, T. Brink, M. Ghidelli, and G. Dehm (2021). Understanding Grain Boundary Electrical Resistivity in Cu: The Effect of Boundary Structure. *ACS Nano*, **15**(10); 16607–16615

Bouzidi, S., M. A. Gdaiem, J. Dhahri, and E. Hlil (2019). Large Magnetocaloric Entropy Change at Room Temperature in Soft Ferromagnetic Manganites. *RSC Advances*, **9**(1); 65–76

Cheng, H., H. Chen, C. Jin, and H. Bai (2023). Modulating the Antiferromagnetic Metallic and Insulating States by Lattice Distortion for Lightly-Doped $La_{0.92}Sr_{0.08}MnO_3$ Films. *Journal of Magnetism and Magnetic Materials*, **565**(January); 170300

Cheng, Z., H. Zhen, A. Li, X. Wang, and H. Kimura (2005). CMR $La_{0.7}Ca_{0.3}MnO_3$ and $La_{0.7}Sr_{0.3}MnO_3$ Thin Films Fabricated by Sol–Gel Method. *Journal of Crystal Growth*, **275**(1-2); e2415–e2419

Çoban Özkan, D., A. Türk, and E. Celik (2021). Synthesis and Characterizations of $LaMnO_3$ Perovskite Powders Using Sol–Gel Method. *Journal of Materials Science: Materials in Electronics*, **32**(11); 15544–15562

Dimri, M. C., H. Khanduri, and R. Stern (2021). Effects of Aliovalent Dopants in $LaMnO_3$: Magnetic, Structural and Transport Properties. *Journal of Magnetism and Magnetic Materials*, **536**(October); 168111

Elmahaishi, M. F., I. Ismail, and F. D. Muhammad (2022). A Review on Electromagnetic Microwave Absorption Properties: Their Materials and Performance. *Journal of Materials Research and Technology*, **20**(September-October); 2188–2220

González García, I., A. Bolarín Miró, O. Rosales González, J. Aguirre Espinosa, C. CortésEsco bedo, and F. Sánchez De Jesús (2023). Effect of Cobalt on the Magnetic Properties and Temperature Coefficient of Resistance for Lanthanum-Strontium Manganite. *Journal of Materials Science: Materials in Electronics*, **34**(29); 1979

He, S., Z. Wang, W. Qiu, H. Zhao, and Y. Lei (2024). Effect of Partial Cation Replacement on Anode Performance of Sodium-Ion Batteries. *Batteries*, **10**(2); 44

Hua, S., P. Zhang, H. Yang, S. Zhang, and H. Ge (2013). The Magnetic and Magnetocaloric Properties of the Perovskite $La_{0.7}Ca_{0.3}Mn_{1-x}Ni_xO_3$. *Journal of Magnetics*, **18**(1); 34–38

Karoblis, D., K. Mazeika, D. Baltrunas, A. Lukowiak, W. Strek, A. Zarkov, and A. Kareiva (2020). Novel Synthetic Approach to the Preparation of Single-Phase $Bi_XLa_{1-X}Mno_{3+\delta}$ Solid Solutions. *Journal of Sol-Gel Science and Technology*, **93**(August); 650–656

Keshri, S., S. Rajput, S. Biswas, L. Joshi, W. Suski, and P. WiŚniewski (2021). Structural, Magnetic and Transport Properties of Ca and Sr Doped Lanthanum Manganites. *Journal of Metals, Materials and Minerals*, **31**(4); 62–68

Khodayari, K. and A. Gholizadeh (2024). Exchange-Spring Behavior in $Ni_{0\cdot3}Cu_{0\cdot2}Zn_{0\cdot5}Fe_2O_4/PbFe_{12}O_{19}$ Nanocomposite. *Physica Scripta*, **99**(3); 035932

Kurniawan, B., N. Sahara, A. Imadudin, I. Rahman, D. Razaq, and D. Munazat (2019). Structure, Microstructure, Electrical Transport Mechanism and Magnetoresistance in $La_{0.8}Ag_{0.2}MnO_3$. In *Journal of Physics: Conference Series*, volume 1402. IOP Publishing, page 066011

Liu, J. W., J. J. Wang, and H. T. Gao (2018). Infrared Emissivities and Microwave Absorption Properties of Perovskite $La_{1-x}Ca_xMnO_3$ ($0 \leq x \leq 0.5$). In *Materials Science Forum*, volume 914. Trans Tech Publ, pages 96–101

Mehner, T., M. Uland, and T. Lampke (2020). Analytical Model to Calculate the Grain Size of Bulk Material Based

on Its Electrical Resistance. *Metals*, **11**(1); 21

Mu, Z., G. Wei, H. Zhang, L. Gao, Y. Zhao, S. Tang, and G. Ji (2022). The Dielectric Behavior and Efficient Microwave Absorption of Doped Nanoscale $LaMnO_3$ at Elevated Temperature. *Nano Research*, **15**(8); 7731–7741

Navas, D., S. Fuentes, A. Castro-Alvarez, and E. Chavez-Angel (2021). Review on Sol-Gel Synthesis of Perovskite and Oxide Nanomaterials. *Gels*, **7**(4); 275

Reddy, A. V., K. Sekhar, N. Dabra, A. Nautiyal, J. S. Hundal, N. Pathak, and R. Nath (2011). Ferroelectric and Magnetic Properties of Hot-Pressed $BiFeO_3$-PVDF Composite Films. *International Scholarly Research Notices*, **2011**(July); 1–5

Rizky, F., S. A. Saptari, A. Tjahjono, and D. S. Khaerudini (2022). Perovskite Manganit Analysis Based on$La_{0.7}Ca_{0.3}Mn_{1-x}Ti_xO_3$ (x= 0, 0.1, 0.2, and 0.3) as Potential Microwave Absorber Material with Sol-Gel Method. *Journal of Physics: Theories and Applications*, **6**(1); 17–24

Saptari, S. A., N. H. Lathifah, A. Tjahjono, and D. Shidqi (2022). Analysis of Crystal Structure and Reflection Loss of Material Based on $La_{0.7}Sr_{0.3}Mn_{1-x}$ (ni, Ti)$_x$/$2O_3$ (x= 0.1, 0.3, and 0.5) Applications for Microwave Absorbers. *Journal of Physics: Theories and Applications*, **6**(2); 106–115

Saradva, A. R. (2023). Radiation impact from Cell Phones and Towers on Human Health and Environment-A Review. *International Journal of Scientific Research in Science and Technology*, **10**(1); 537–541

Suresh, S., P. Vindhya, S. Devika, and V. Kavitha (2023). Structural, Optical and Dielectric Properties of Nanostructured $La_{1-x}Sr_xMnO_3$ Perovskites. *Materials Today Communications*, **36**(August); 106657

Taşarkuyu, E., A. Coşkun, A. Irmak, S. Aktürk, G. Ünlü, Y. Samancıoğlu, A. Yücel, C. Sarıkürkçü, S. Aksoy, and M. Acet (2011). Effect of High Temperature Sintering on the Structural and the Magnetic Properties of $La_1 \cdot_4 Ca_1 \cdot_6 Mn_2O_7$. *Journal of Alloys and Compounds*, **509**(9); 3717–3722

Ulyanov, A. N., Y. M. Kang, S. I. Yoo, D. S. Yang, H. M. Park, K. W. Lee, and S. C. Yu (2006). Local Structure and Electron Configuration Effects on Curie Temperature in $La_{0.7}Ca_{0.3}Mn_{1-x}Ti_xO_3$ Lanthanum Manganites. *Journal of Magnetism and Magnetic Materials*, **304**(1); e331–e333

Xu, H., H. Zhang, Y. Ma, M. Jiang, Y. Zhang, Y. Wu, H. Zhang, R. Xia, Q. Niu, and X. Li (2019). Morphology Control of Organic Halide Perovskites by Adding $BiFeO_3$ Nanostructures for Efficient Solar Cell. *Scientific Reports*, **9**(1); 15441

Ye, X., S. Dong, X. Jin, J. Wei, L. Wang, and Y. Zhang (2022). Enhancement in the Electrochemical Performance of Strontium (sr)-Doped $LaMnO_3$ As Supercapacitor Materials. *Coatings*, **12**(11); 1739

Zhang, F., Y. Chen, Y. Ren, Q. Zheng, L. Wang, and W. Jiang (2022). Anionic MOF Derived Bimetallic NixCoy@ Nano-Porous Carbon Composites toward Strong and Efficient Electromagnetic Wave Absorption. *Journal of Materiomics*, **8**(4); 852–862

Zhang, H. G., Y. J. Zhang, W. H. Wang, and G. H. Wu (2011). Origin of the Constricted Hysteresis Loop in Cobalt Ferrites Revisited. *Journal of Magnetism and Magnetic Materials*, **323**(15); 1980–1984

Zhang, S. and Q. Cao (2012). Electromagnetic and Microwave Absorption Performance of Some Transition Metal Doped $La_{0.7}Sr_{0.3}Mn_{1-x}TM_xO_{3\pm\delta}$ (TM= Fe, Co or Ni). *Materials Science and Engineering: B*, **177**(9); 678–684

Zheng, J., H. Zhao, X. Guo, X. Jin, L. Wang, S. Dong, and J. Chen (2023). Enhanced Electrochemical Performance of $LaMnO_3$ Nanoparticles by Ca/Sr Doping. *Coatings*, **14**(1); 20

